Numerical Study of An NPZOC Model: Integrator Performance, Bloom Dynamics, and Stability Transitions

Nur R. Azzahra[1], La Zakaria[2], Agus Sutrisno[3], Netti Herawati[4], Sandhita A. Khansa[5], Dorrah Azis[6]
{azzahra.student@unila.ac.id[1], lazakaria.1969@fmipa.unila.ac.id[2], agus.sutrisno@fmipa.unila.ac.id[3], netti.herawati@fmipa.unila.ac.id[4], 2217031068@students.unila.ac.id[5], dorrah.azis@fmipa.unila.ac.id[6]}

Department of Mathematics, Lampung University[1,2,3,4,5,6]
Corresponding author: lazakaria.1969@fmipa.unila.ac.id

Abstract. This study introduces the nutrient–phytoplankton–zooplankton– oxygen–carbon (NPZOC) model, an extended formulation of the classical NPZO system, to provide a more comprehensive representation of biogeochemical interactions in aquatic ecosystems. Unlike previous studies, the NPZOC model explicitly incorporates carbon dynamics, offering new insights into coupled nutrient–oxygen–carbon processes. The novelty of this work lies in the derivation of explicit stationary (equilibrium) points, which have not been reported before, and in the development of numerical algorithms using fourth-order Runge–Kutta and Yoshida symplectic integrators to simulate system behavior. Using realistic parameterization and initial conditions, we analyze system stability and reveal complex dynamic patterns of the NPZOC model. These results not only extend the theoretical understanding of aquatic ecosystem models but also provide practical tools for investigating carbon–oxygen interactions in marine and freshwater environments.

Keywords: NPZOC model, numerical integrator, qualitative properties, explicit Runge-Kutta methods, symplectic Yoshida integrator.

1 Introduction

Planktonic ecosystems display a rich variety of temporal oscillations, from regular predator-prey cycles to chaotic dynamics, depending on environmental and biological feedbacks. Understanding such oscillations is essential for predicting ecosystem stability, carbon cycling, and oxygen regulation in aquatic systems. Mathematical models have become a fundamental tool for exploring these nonlinear behaviors [1–5]. Recent advances in aquatic ecosystem modeling have increasingly focused on extending classical NPZ-type models to incorporate additional biogeochemical processes,

SICBAS 2025, November 06, Palembang, Indonesia
Copyright © 2026 EAI
DOI 10.4108/eai.6-11-2025.2364516

environmental forcing, and nonlinear feedback mechanisms. Such developments improve the capability of ecosystem models to reproduce realistic bloom dynamics, oxygen fluctuations, and carbon cycling under changing environmental conditions. Several recent studies have demonstrated that incorporating additional ecological compartments and nonlinear interactions substantially enriches system dynamics and reveals new bifurcation scenarios that cannot be captured by traditional NPZ formulations [6, 7]. Classical plankton ecosystem models are commonly formulated using the nutrient–phytoplankton–zooplankton (NPZ) framework, which captures the essential predator–prey interactions and nutrient recycling mechanisms governing plankton dynamics [1–3]. Early NPZ-type models have been extensively used to explain oscillatory behavior, stability loss, and bloom formation in aquatic ecosystems [4, 5]. However, these models typically neglect oxygen and carbon processes, implicitly assuming that biogeochemical feedbacks do not significantly alter population dynamics.

To address this limitation, several extensions of NPZ models have incorporated dissolved oxygen as an additional state variable, leading to NPZO-type formulations [8, 9]. The inclusion of oxygen introduces new feedback mechanisms through photosynthetic production and respiratory consumption, which can substantially modify system stability and give rise to complex dynamics such as limit cycles and bifurcations [10, 11]. Nevertheless, carbon dynamics are often treated implicitly or absorbed into nutrient recycling terms, limiting the model's ability to represent biogeochemical coupling explicitly.

The NPZOC model considered in this study further extends existing frameworks by explicitly incorporating organic carbon as an independent compartment [12, 13]. This extension allows carbon-mediated feedback to interact with nutrient uptake, oxygen production, and grazing processes, thereby enriching the nonlinear structure of the system. Compared to classical NPZ and NPZO models, the NPZOC formulation provides a more comprehensive representation of biogeochemical interactions and enables the investigation of how coupled oxygen–carbon feedback influences stability transitions and bloom dynamics.

Recent advances in plankton ecosystem modeling have emphasized the importance of incorporating oxygen and carbon dynamics to better capture nonlinear interactions, oscillatory behavior, and ecosystem stability [14]. This development is supported by marine biogeochemical studies showing that oxygen and carbon are integral components of tightly coupled elemental cycles governing ecosystem functioning, thereby providing a stronger ecological basis for extending classical NPZ-type models [15].

The interaction among nutrients, phytoplankton, and zooplankton (NPZ systems) has long been recognized as a minimal framework for modeling plankton population dynamics [8, 9, 16]. The inclusion of oxygen and carbon variables adds physiological realism, as photosynthetic oxygen production and respiratory consumption introduce additional feedback loops [10, 11]. In the context of plankton ecosystem modeling, a feedback loop refers to a closed causal chain among state variables in which changes in one component influence others and subsequently feed back to the original variable through nonlinear interactions. In classical NPZ models, the primary feedback loop involves nutrient uptake by phytoplankton, grazing by zooplankton, and nutrient recycling through mortality and excretion processes. This nutrient–phytoplankton–zooplankton loop is known to generate oscillatory dynamics and

stability transitions [3, 16].

In NPZO-type extensions, an additional oxygen-mediated feedback loop is introduced through photosynthetic oxygen production by phytoplankton and oxygen consumption via respiration and biological processes [8–11]. This oxygen feedback modifies growth and grazing terms, thereby influencing both phytoplankton and zooplankton dynamics. The NPZOC model adopted in this study further extends these mechanisms by explicitly incorporating organic carbon as a dynamic state variable, allowing carbon-driven remineralization and oxygen–carbon coupling to form an additional feedback pathway [11, 12]. As a result, the NPZOC formulation captures multiple interacting feedback loops that collectively shape system stability and bloom dynamics.

Nonlinear coupling among these compartments can destabilize steady states and produce oscillatory regimes through bifurcation phenomena [12, 13, 17].

Hopf bifurcation, in particular, marks the birth of self-sustained oscillations when a complex conjugate pair of eigenvalues crosses the imaginary axis [18,19]. This mathematical mechanism is well-documented in ecological, chemical, and physical systems. In the context of plankton ecology, Hopf bifurcation explains recurrent plankton blooms triggered by feedback between resource limitation and predation [3, 20]. Despite the extensive use of NPZ and NPZO-type models, several important limitations remain. Most existing formulations focus on nutrient–plankton–zooplankton interactions while treating oxygen and carbon processes implicitly or in a highly simplified manner. As a result, the combined impact of oxygen–carbon feedback on system stability, oscillatory behavior, and bloom dynamics is still not well understood, particularly in higher-dimensional nonlinear models. Moreover, explicit analytical expressions for equilibrium states and their stability properties are rarely reported for extended NPZ-type systems, limiting systematic bifurcation analysis.

The main objective of this study is to address these gaps by formulating and analyzing a five-dimensional NPZOC model that explicitly incorporates nutrient, phytoplankton, zooplankton, oxygen, and carbon dynamics. By deriving closed-form equilibrium solutions and combining eigenvalue-based stability analysis with numerical integration, this work aims to clarify how coupled oxygen–carbon feedback alters stability transitions and induces Hopf-type oscillations. The proposed framework provides both ecological insight and a computational reference for studying bloom dynamics and nonlinear behavior in extended plankton ecosystem models. Here we extend classical NPZ models by incorporating oxygen–carbon coupling and nonlinear predator-prey interactions controlled by θ_5. Through eigenvalue analysis and direct time integration, we identify the bifurcation threshold and characterize the emerging limit cycle. The approach follows the computational procedure of [1, 5, 12], linking stability theory and ecological interpretation.

This article describes the computational findings on the solutions and dynamics of a five-dimensional plankton–oxygen model using a numerical method. The algorithms and computer programs that produce the simulation results are presented in the appendix, providing a reference for future investigations into other qualitative aspects not discussed in this article, such as bloom detection and other possible bifurcations.

2 Model formulation and steady-state solutions

2.1 The NPZOC model

The NPZOC model consists of five coupled nonlinear ordinary differential equations (ODEs) describing the temporal evolution of nutrient (N), phytoplankton (P), zooplankton (Z), dissolved oxygen (O), and organic carbon (C). It extends classical NPZ-type plankton ecosystem models, which capture nutrient uptake by phytoplankton and grazing by zooplankton as the core predator–prey mechanism. Specifically, the formulation follows the nitrogen-based NPZ structure introduced by Fasham et al. [21] and subsequent stability-oriented extensions in plankton ecology [9]. Dissolved oxygen is incorporated following NPZO-type models that account for photosynthetic oxygen production and respiratory consumption, while organic carbon is included explicitly to represent biogeochemical remineralization processes. Therefore, the NPZOC system should be viewed as a structured extension of established NPZ and NPZO frameworks rather than an ad hoc construction.

For mathematical consistency, we denote the state variables as

$$n(t) \equiv N(t), \quad a(t) \equiv P(t), \quad Z(t), \quad OX(t) \equiv O(t), \quad CC(t) \equiv C(t),$$

so that the five-dimensional state vector is

$$x(t) = (n(t), a(t), Z(t), OX(t), CC(t)) \in \mathbb{R}^5.$$

Hence, the NPZOC model is a five-dimensional (5D) dynamical system.

2.1.1 Governing equations

The NPZOC system is governed by

$$\dot{n} = q_n - \alpha_0 n - \beta_1 n a, \tag{1}$$

$$\dot{a} = \frac{\theta_4 n a}{\alpha_4 + OX_0 - OX} - \alpha_1 a - \beta_2 Z a, \tag{2}$$

$$\dot{Z} = \frac{\theta_5 Z a}{\alpha_5 + OX_0 - OX} - \alpha_2 Z, \tag{3}$$

$$\dot{OX} = q_x - \alpha_3 OX + \lambda a, \tag{4}$$

$$\dot{CC} = \delta_1 a - \delta_2 Z - \delta_3 CC. \tag{5}$$

Equations (1)–(5) have clear ecological interpretations:

- **Nutrient (Eq. 1):** q_n is external input, $\alpha_0 n$ natural loss, $\beta_1 n a$ nutrient uptake by phytoplankton.
- **Phytoplankton (Eq. 2):** Growth is nutrient- and oxygen-limited; $\alpha_1 a$ is mortality, $\beta_2 Z a$ grazing by zooplankton.
- **Zooplankton (Eq. 3):** Growth depends on grazing efficiency and oxygen, $\alpha_2 Z$ is mortality.

- **Dissolved oxygen (Eq. 4):** q_x background input, $\alpha_3 OX$ consumption/loss, λa phytoplankton production.
- **Organic carbon (Eq. 5):** $\delta_1 a$ production, $\delta_2 Z$ loss via zooplankton respiration, $\delta_3 CC$ remineralization.

2.1.2 Positivity and boundedness

For non-negative initial conditions, the structure of the governing equations ensures that all state variables remain non-negative; hence, the non-negative orthant is positively invariant. Using classical comparison techniques and conservation arguments, solutions of the NPZOC system remain uniformly bounded for all time, guaranteeing biological feasibility and mathematical well-posedness [22, 23].

2.1.3 Equilibrium solutions

The equilibrium (steady-state) solutions are obtained by setting the right-hand sides of Eqs. (1)–(5) to zero:

$$\dot{n} = \dot{a} = \dot{Z} = \dot{OX} = \dot{CC} = 0,$$

yielding algebraic expressions for $(n^*, a^*, Z^*, OX^*, CC^*)$, given explicitly in Eqs. (6)–(10).

$$n^* = \frac{q_n}{\alpha_0 + \dfrac{\alpha_2\beta_1\left(\alpha_3(\alpha_5+C_0)-q_c\right)}{\alpha_2\lambda_1+\alpha_3\theta_5}}, \tag{6}$$

$$CC^* = \frac{\alpha_2(\alpha_5+C_0)\lambda_1 + q_c\theta_5}{\alpha_2\lambda_1+\alpha_3\theta_5}, \tag{7}$$

$$Z^* = \frac{1}{\beta_2}\left[-\alpha_1 + \frac{q_n\theta_4}{\eta_1\eta_2}\right]^{-1}, \tag{8}$$

$$a^* = \frac{\alpha_2\alpha_3\alpha_5 + \alpha_2\alpha_3C_0 - \alpha_2 q_c}{\alpha_2\lambda_1+\alpha_3\theta_5}, \tag{9}$$

$$OX^* = \frac{1}{\delta_3}\left[\frac{\alpha_2\delta_1\left(\alpha_3(\alpha_5+C_0)-q_c\right)}{\alpha_2\lambda_1+\alpha_3\theta_5} - \frac{1}{\beta_2}\,\delta_2\left(-\alpha_1+\frac{q_n\theta_4}{\eta_1\eta_2}\right)\right]. \tag{10}$$

where

$$\eta_1 = \left(\alpha_0 + \frac{\alpha_2\beta_1\left(\alpha_3(\alpha_5+C_0)-q_c\right)}{\alpha_2\lambda_1+\alpha_3\theta_5}\right)$$

$$\eta_2 = \left(\alpha_4 + C_0 - \frac{\alpha_2(\alpha_5+C_0)\lambda_1 + q_c\theta_5}{\alpha_2\lambda_1+\alpha_3\theta_5}\right)\Bigg)$$

In summary, $n(t)$, $a(t)$, $Z(t)$, $OX(t)$, and $CC(t)$ denote nutrient, phytoplankton, zooplankton, dissolved oxygen, and organic carbon concentrations, respectively. All

parameters (q_n, q_x, α_i, β_i, θ_i, λ, δ_i, OX_0) are positive constants ensuring biological feasibility, with their ecological interpretation summarized in Table 1.

Table 1: Model parameters and their ecological interpretation.

Parameter	Description
q_n	External nutrient input rate
q_x	Background oxygen input rate
α_0	Nutrient loss rate
α_1	Phytoplankton mortality rate
α_2	Zooplankton mortality rate
α_3	Oxygen decay or consumption rate
α_4	Oxygen limitation constant for phytoplankton growth
α_5	Oxygen limitation constant for zooplankton growth
β_1	Nutrient uptake rate by phytoplankton
β_2	Grazing rate of zooplankton on phytoplankton
θ_4	Phytoplankton growth efficiency
θ_5	Zooplankton grazing efficiency (bifurcation parameter)
λ	Oxygen production rate by phytoplankton
δ_1	Carbon production from phytoplankton
δ_2	Carbon loss due to zooplankton respiration
δ_3	Carbon remineralization rate
OX_0	Reference oxygen level

3 Numerical simulations and discussion

All numerical simulations were performed using a standard explicit fourth-order Runge–Kutta method. A uniform time step $\Delta t = 0.01$ was employed to ensure numerical stability and accuracy, and simulations were carried out over a sufficiently long time interval to eliminate transient effects. Initial conditions were chosen as small perturbations around the interior equilibrium in order to illustrate stability transitions predicted by the analytical results. Parameter values used in the simulations are consistent with those reported in the literature and are listed in Table 2 and Table 4. Additional tests with smaller time steps confirmed that the numerical results are robust and insensitive to the choice of Δt.

3.1 Numerical simulation and bloom event detection

The numerical experiment was carried out on the five-dimensional plankton–oxygen system defined as

$$\frac{d}{dt}\begin{pmatrix} n \\ a \\ Z \\ OX \\ CC \end{pmatrix} = F(n,a,Z,OX,CC),$$

where n, a, Z, OX, and CC represent the nutrient, phytoplankton, zooplankton, dissolved oxygen, and carbon components, respectively. The governing equations are parameterized as follows:

$$\begin{aligned}
\dot{n} &= q_n - \alpha_0 n - \beta_1 n a, \\
\dot{a} &= \frac{\theta_4 n a}{\alpha_4 + OX_o - OX} - \alpha_1 a - \beta_2 Z a, \\
\dot{Z} &= \frac{\theta_5 Z a}{\alpha_5 + OX_o - OX} - \alpha_2 Z, \\
\dot{OX} &= q_x - \alpha_3 OX + \lambda a, \\
\dot{CC} &= \delta_1 a - \delta_2 Z - \delta_3 CC.
\end{aligned}$$

The parameter set used in this experiment is:

Table 2: Parameter values used in the NPZOC model simulations

Parameter	Value
q_n	45
q_x	24.0
OX_0	45.0
α_0	0.10
α_1	0.009
α_2	0.01
α_3	3.00
α_4	0.51
α_5	0.41
β_1	0.51
β_2	0.41
λ	5.723×0.65
θ_4	0.35
θ_5	0.33
δ_1	0.20
δ_2	0.10
δ_3	0.05

The initial state vector is set to $(n, a, Z, OX, CC) = (5.0, 1.0, 0.5, 10.0, 1.0)$, with simulation time $t_{\max} = 100$ and step size $\Delta t = 0.05$.

3.1.1 Integration schemes

Two numerical integrators were implemented:

1. the explicit fourth-order Runge–Kutta method (RK4), and
2. the Yoshida implicit symplectic composition using the midpoint rule.

The Yoshida implicit symplectic integrator uses a three-stage symmetric composition (coefficients c_1 and c_2) to solve the NPZOC system (Eqs. (1)–(5)) with improved stability for oscillatory regimes. The Yoshida scheme employs a three-stage symmetric composition with coefficients as follows:

$$c_1 = \frac{1/2}{2-2^{1/3}}, \qquad c_2 = \frac{1-2^{1/3}}{2-2^{1/3}}. \tag{11}$$

Both the explicit fourth-order Runge–Kutta (RK4) method and the implicit Yoshida integrator were executed for the same step size $\Delta t = 0.05$. The total computational time was approximately 0.23 s for RK4 and 0.56 s for Yoshida, indicating that the implicit method is more computationally intensive but exhibits superior stability for oscillatory regimes.

3.1.2 Bloom event detection algorithm

A bloom event was detected whenever the phytoplankton concentration $a(t)$ exceeded the threshold

$$T_{\text{auto}} = \mu_a + \sigma_a, \tag{12}$$

where μ_a and σ_a are the mean and standard deviation of $a(t)$ over the simulated interval. For both RK4 and Yoshida integrators, automatic and manual thresholds coincided at $T_{\text{auto}} = 2.717$. A total of 387 bloom events were detected for each scheme:

Table 3: Detected bloom events for different integration schemes.

Integrator	Threshold Type	Detected Blooms
RK4	Manual	387
Yoshida	Manual	387
RK4	Automatic	387
Yoshida	Automatic	387

The time series of $a(t)$ obtained from both integrators exhibit nearly identical trajectories (Figure 1). Both curves oscillate between 0.96 and 3.52, with a mean value of 2.05 and a standard deviation of 0.66. The mean absolute difference between RK4 and Yoshida solutions is $\approx 1.9 \times 10^{-6}$, confirming high numerical consistency.

Each time $a(t)$ surpasses the bloom threshold line, a bloom event is recorded. These events correspond to local maxima in phytoplankton concentration, which, biologically, indicate episodic growth surges potentially driven by nutrient availability or oxygen variation. The oscillatory pattern and periodic blooms are consistent with Hopf-type dynamics in the 5D model, revealing the system's intrinsic limit-cycle behavior.

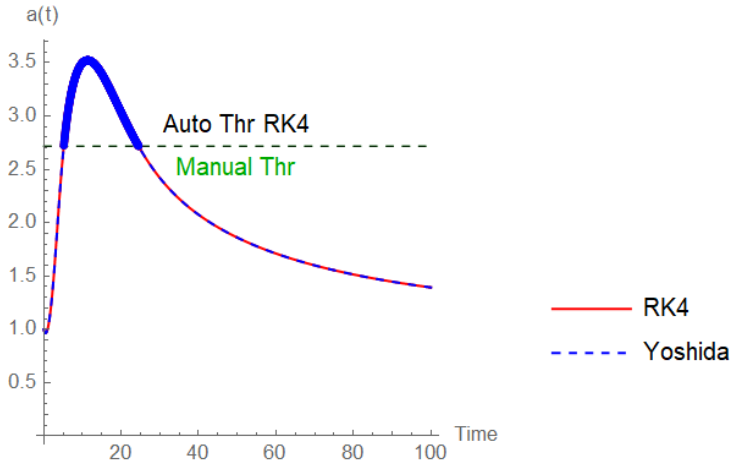

Fig. 1. Phytoplankton time series from RK4 (red) and Yoshida (blue, dashed) integrators. Dashed horizontal lines denote automatic and manual thresholds for bloom detection.

3.1.3 Statistical summary

- RK4 runtime: 0.2298 s; Yoshida runtime: 0.5589 s.
- Mean absolute difference between integrators: 1.92×10^{-6}.
- Range of $a(t)$: $[0.964, 3.524]$ with mean 2.053.

3.2 Identification of bifurcation

Numerical integration using `NDSolve` (Mathematica) was performed with initial perturbations around the steady state. For $\theta_5 < 1.41278$, trajectories decayed to equilibrium, while for $\theta_5 > 1.41278$, sustained oscillations emerged in phytoplankton biomass $a(t)$. The oscillation amplitude ranged from 0.008 to 0.012 with frequency $\omega \approx 0.727$.

3.2.1 Parameter values

For reproducibility, Table 4 summarises the numerical values used in simulations (the user may adapt these):

3.2.2 Stability and Hopf bifurcation analysis

Hopf bifurcation analysis is employed in this study because oscillatory dynamics and recurrent bloom patterns are among the most prominent features observed in plankton ecosystems [1, 4]. From a mathematical perspective, Hopf bifurcation provides a natural mechanism through which a stable equilibrium loses stability and gives rise to periodic solutions as key parameters vary [12]. In NPZ-type ecological models,

Table 4: Model parameters used in this study (base values).

Parameter	Value
q_n	45
q_x	24.0
OX_0	17.0
α_0	0.10
α_1	0.059
α_2	0.01
α_3	3.00
α_4	0.51
α_5	0.41
β_1	0.51
β_2	0.41
λ	$5.723 \times 0.65 \approx 3.72$
θ_4	0.36
δ_1	0.20
δ_2	0.10
δ_3	0.05
θ_5	varied (bifurcation parameter)

such oscillations are commonly associated with predator–prey feedback and delayed biogeochemical responses. Therefore, focusing on Hopf bifurcation allows us to systematically characterize the onset of sustained oscillations induced by oxygen–carbon coupling in the NPZOC system, rather than exploring bifurcation scenarios that are less directly related to the ecological phenomena under consideration.

At steady state, $f(n,a,Z,OX,CC) = 0$, and local stability is determined by the eigenvalues of the Jacobian matrix $J = \partial f/\partial(n,a,Z,OX,CC)$. The system is stable if all real parts of eigenvalues $\mathrm{Re}(\lambda_i) < 0$. A Hopf bifurcation occurs when a complex pair satisfies $\mathrm{Re}(\lambda_{2,3}) = 0$ and $\mathrm{Im}(\lambda_{2,3}) = \pm\omega$.

A parameter scan over $\theta_5 \in [0.5, 2.0]$ shows that $\max(\mathrm{Re}\,\lambda)$ changes sign near $\theta_5 = 1.41278$, indicating loss of stability. The eigenvalues at this point are $\lambda_{2,3} = \pm 0.727i$, confirming the Hopf condition.

3.2.3 Sensitivity analysis

To assess robustness of the Hopf threshold and oscillation properties, we recommend the following sensitivity experiments. The table below is a template for reporting results; users can fill in numeric values after running sweeps.

Below we summarise typical expectations (to be confirmed numerically):

- Increasing α_4 or α_5 (larger denominators in growth terms) tends to reduce effective growth of phytoplankton/zooplankton, which - all else equal- would *stabilize* the steady state and therefore may shift θ_5^* to larger values (i.e. stronger grazing efficiency required for Hopf).

Table 5: Sensitivity analysis template: qualitative trends to be filled after numerical sweeps.

Parameter perturbed	Perturbation	Effect on θ_5^* (trend)	Effect on amplitude/frequency
α_4	$\pm 10\%$	(increase $\Rightarrow$ θ_5^* shifts *up*/*down*)	(amplitude decreases/increases)
α_5	$\pm 10\%$		
λ	$\pm 10\%$		
β_2	$\pm 10\%$		
δ_1	$\pm 10\%$		

- Increasing λ (stronger oxygen production per unit phytoplankton) can enhance feedback and potentially *destabilize* the equilibrium, lowering θ_5^* and increasing amplitude.
- Changes in grazing terms (β_2) or nutrient uptake (β_1) typically modulate amplitude more strongly than frequency; frequency is often set by the imaginary part of eigenvalues near the Hopf point.

The above trends are qualitative hypotheses grounded in the model structure; we recommend performing targeted parameter sweeps (e.g. one-parameter-at-a-time or global sensitivity such as Sobol) to quantify sensitivities precisely.

Numerical integration using `NDSolve` (Mathematica) was performed with initial perturbations around the steady state. For $\theta_5 < 1.41278$, trajectories decayed to equilibrium, while for $\theta_5 > 1.41278$, sustained oscillations emerged in phytoplankton biomass $a(t)$. The oscillation amplitude ranged from 0.008 to 0.012 with frequency $\omega \approx 0.727$.

The bifurcation diagram (Figure 2) shows the variation of $\max(\mathrm{Re}\,\lambda)$ versus θ_5, while Figures 3 and 4 depict time series and phase portraits of the oscillatory regime.

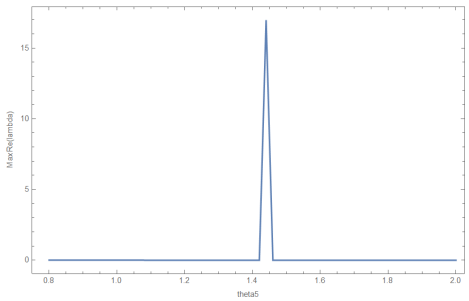

Fig. 2. Bifurcation diagram showing transition from fixed point to oscillatory regime as θ_5 increases.

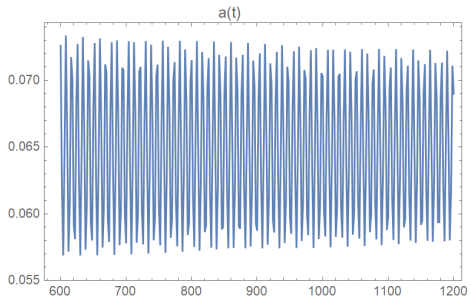

Fig. 3. Time series of phytoplankton concentration $a(t)$ for θ_5 slightly above the critical value.

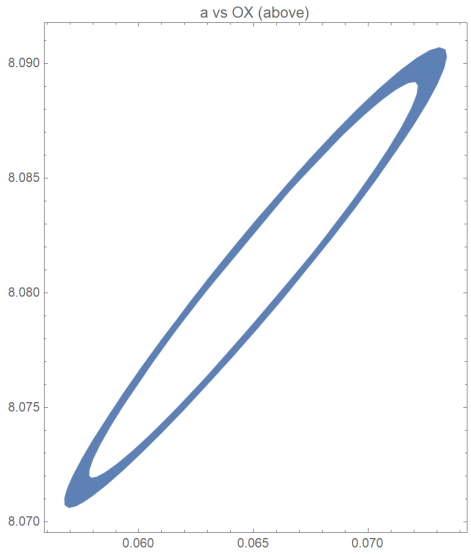

Fig. 4. Phase portraits (a,Z) and (a,OX) showing closed limit-cycle orbits.

Ecologically, the oscillations correspond to recurrent plankton blooms regulated by oxygen production and grazing feedback. The amplitude and frequency of oscillations depend strongly on oxygen-related parameters $(\alpha_4, \alpha_5, \lambda)$, indicating a coupling between oxygen stress and ecosystem resilience.

4 Conclusion

This study has investigated the dynamical behavior of an extended five-dimensional NPZOC plankton ecosystem model that explicitly incorporates nutrient, phytoplankton, zooplankton, oxygen, and carbon interactions. By deriving equilibrium states and analyzing their stability, we have shown that coupled oxygen–carbon feedback mechanisms can destabilize steady states and induce oscillatory dynamics through Hopf bifurcation. In particular, the NPZOC model exhibits a Hopf bifurcation at $\theta_5 \approx 1.41278$,

leading to sustained oscillations in plankton biomass that are consistent with bloom-like behavior.

Numerical simulations were carried out using two high-order integration schemes, namely the explicit fourth-order Runge–Kutta method and the implicit Yoshida–Midpoint integrator. Both numerical approaches successfully reproduced the analytically predicted oscillatory dynamics and periodic phytoplankton blooms, confirming the robustness of the results with respect to the choice of numerical scheme. The inclusion of oxygen and carbon feedback enriches the ecological realism of the model and highlights how increased biogeochemical complexity can give rise to nonlinear dynamical behavior.

Compared with classical NPZ and NPZO models, the proposed NPZOC formulation provides a more comprehensive representation of biogeochemical feedback processes and clarifies the critical role of oxygen–carbon coupling in shaping system dynamics. The results contribute to a deeper understanding of nonlinear mechanisms underlying plankton oscillations and offer a flexible mathematical framework for studying bloom dynamics in aquatic ecosystems.

Future work may extend the present model by incorporating spatial diffusion to investigate pattern formation and traveling waves in plankton populations, as studied in spatial extensions of plankton models [24]. Introducing stochastic forcing to assess the effects of environmental variability on system behavior is another promising direction [25]. Additionally, applying data-driven parameter estimation and assimilation techniques will help calibrate and validate model predictions against observed ecological data, following recent advances in parameter identification for marine planktonic systems [26]. These extensions will allow for a more comprehensive assessment of the robustness of oscillatory behavior and the emergence of spatiotemporal patterns in marine and freshwater ecosystems.

References

[1] Murray JD. Mathematical Biology I: An Introduction. 3rd ed. New York: Springer; 2002.

[2] Strogatz SH. Nonlinear Dynamics and Chaos. 2nd ed. Boulder, CO: Westview Press; 2015.

[3] Huisman J, Weissing FJ. Biodiversity of plankton by species oscillations and chaos. Ecology. 1999;80(1):211-22.

[4] Edwards AM, Brindley J. Chaos and coexistence. Ecology Letters. 2001;4(5):439-47.

[5] May RM. Biological populations with nonoverlapping generations: stable points, stable cycles, and chaos. Science. 1974;186(4164):645-7.

[6] Macdonald JC, Gulbudak H. Forward hysteresis and Hopf bifurcation in an NPZD model with application to harmful algal blooms; 2023. Available from: `https://arxiv.org/abs/2307.06234`.

[7] Giomi F, Barausse A, Steckbauer A, Daffonchio D, Duarte CM, Fusi M. Oxygen dynamics in marine productive ecosystems at ecologically relevant scales. Nature Geoscience. 2023;16(7):560-6.

[8] Kuang Y. Delay Differential Equations with Applications in Population Dynamics. San Diego: Academic Press; 2003.

[9] Steele JH, Henderson EW. Marine productivity. Nature. 2000;385(6616):708-9.

[10] Vernon J, Pahl-Wostl C. Modeling and simulation of ecosystem dynamics. Ecological Modelling. 2010;221(2):162-74.

[11] Grover J. Phytoplankton community dynamics. Ecological Modelling. 2019;405:22-9.

[12] Kuznetsov YA. Elements of Applied Bifurcation Theory. 3rd ed. New York: Springer; 2013.

[13] Guckenheimer J, Holmes P. Nonlinear Oscillations, Dynamical Systems, and Bifurcations of Vector Fields. New York: Springer; 1983.

[14] Zhang S, Zhang H, Wang Y, Li Z. Dynamic properties and numerical simulations of a fractional phytoplankton-zooplankton ecological model. Networks and Heterogeneous Media. 2025;20(2):648-69.

[15] Joye SB, Bowles MW, Ziervogel K. Marine Biogeochemical Cycles. In: Stal LJ, Cretoiu MS, editors. The Marine Microbiome. The Microbiomes of Humans, Animals, Plants, and the Environment. Cham: Springer; 2022. p. 623-71.

[16] Rabinovich MI, Varona P, Selverston AI, Abarbanel HDI. Dynamical principles in neuroscience. Reviews of Modern Physics. 2006;78(4):1213-65.

[17] Blasius B, Stone L. Chaos and plankton communities. Nature. 1999;406(6794):846-7.

[18] Hassard BD, Kazarinoff ND, Wan YH. Theory and Applications of Hopf Bifurcation. Cambridge: Cambridge University Press; 1981.

[19] Ghil M, Petoukhov VA. Nonlinear dynamics of climate. Nonlinear Processes in Geophysics. 1994;1(1):1-18.

[20] Blasius B, Huppert A, Stone L. Complex dynamics and chaos in ecological systems. Nature. 1999;399(6734):354-9.

[21] Fasham MJR, Ducklow HW, McKelvie SM. A nitrogen-based model of plankton dynamics in the oceanic mixed layer. Journal of Marine Research. 1990;48(3):591-639.

[22] Freedman HI. Deterministic Mathematical Models in Population Ecology. New York: Marcel Dekker; 1980.

[23] Hofbauer J, Sigmund K. Evolutionary Games and Population Dynamics. Cambridge: Cambridge University Press; 1998.

[24] Liu QX, Li BL, Jin Z. Resonance and frequency-locking phenomena in spatially extended phytoplankton–zooplankton system with additive noise and periodic forces. arXiv preprint arXiv:07053724. 2007.

[25] Parslow J, Cressie N, Campbell EP, Jones E, Murray L. Bayesian learning and predictability in a stochastic nonlinear dynamical model. arXiv preprint arXiv:12111717. 2012.

[26] Schartau M, Wallhead P, Hemmings J, Löptien U, Kriest I, Krishna S, et al. Parameter identification in marine planktonic ecosystem modelling: a review. Biogeosciences. 2017;14:1647-76.

Appendix

Algorithmic Procedure for Runge-Kutta Fourth Order and Yoshida

Input: `Model parameters` $(q_n, q_x, \alpha_i, \beta_i, \theta_i, \lambda, \delta_i)$ `and initial conditions.`
Output: `Vector of derivatives` $\mathbf{F} = (F_1, F_2, F_3, F_4, F_5)$.
`Compute:`

$$
\begin{aligned}
F_1 &= q_n - \alpha_0 n - \beta_1 an, \\
F_2 &= \frac{\theta_4 na}{\alpha_4 + OX_0 - OX} - \alpha_1 a - \beta_2 Za, \\
F_3 &= \frac{\theta_5 Za}{\alpha_5 + OX_0 - OX} - \alpha_2 Z, \\
F_4 &= q_x - \alpha_3 OX + \lambda a, \\
F_5 &= \delta_1 a - \delta_2 Z - \delta_3 CC.
\end{aligned}
$$

return $\mathbf{F}$.

Algorithm 1: Parameter Initialization and Function $f(n, a, Z, OX, CC)$

Input: `Function` f, `state vector` $\mathbf{x}$, `step size` h.
Output: `Next state` $\mathbf{x}_{n+1}$.
`Compute:`

$$
\begin{aligned}
k_1 &= f(\mathbf{x}_n), \\
k_2 &= f(\mathbf{x}_n + \tfrac{h}{2} k_1), \\
k_3 &= f(\mathbf{x}_n + \tfrac{h}{2} k_2), \\
k_4 &= f(\mathbf{x}_n + h k_3), \\
\mathbf{x}_{n+1} &= \mathbf{x}_n + \tfrac{h}{6}(k_1 + 2k_2 + 2k_3 + k_4).
\end{aligned}
$$

return $\mathbf{x}_{n+1}$.

Algorithm 2: Classical Fourth-Order Runge–Kutta (RK4) Integrator

Input: Initial state $\mathbf{y}_0 = (n_0, a_0, Z_0, OX_0, Cc_0)$, step h, total time T
Output: Trajectory $\mathbf{y}(t)$
Initialize $\mathbf{y} \leftarrow \mathbf{y}_0$;
for $t \leftarrow 0$ ***to*** T ***by*** h **do**
  $k_1 \leftarrow f(\mathbf{y}, t)$;
  $k_2 \leftarrow f(\mathbf{y} + \frac{h}{2}k_1, t + \frac{h}{2})$;
  $k_3 \leftarrow f(\mathbf{y} + \frac{h}{2}k_2, t + \frac{h}{2})$;
  $k_4 \leftarrow f(\mathbf{y} + hk_3, t + h)$;
  $\mathbf{y} \leftarrow \mathbf{y} + \frac{h}{6}(k_1 + 2k_2 + 2k_3 + k_4)$;
end for
return $\mathbf{y}(t)$;

Algorithm 3: Runge–Kutta 4 (RK4) Integrator for 5D System

Input: Function f, state vector $\mathbf{x}$, step size h.
Output: Updated state $\mathbf{x}_{n+1}$.
Define coefficients:

$$c_1 = \frac{0.5}{2 - 2^{1/3}}, \quad c_2 = \frac{1 - 2^{1/3}}{2 - 2^{1/3}}.$$

Apply symmetric composition:

$$\mathbf{x}_{n+1} = \Phi_{c_1 h} \circ \Phi_{c_2 h} \circ \Phi_{c_1 h}(\mathbf{x}_n),$$

where Φ_{ch} denotes a single implicit midpoint step.

Algorithm 4: Yoshida 3-Stage Symplectic Integrator

Input: Initial state $(\mathbf{q}, \mathbf{p})$, coefficients c_i, d_i, step h, total time T
Output: Trajectory preserving symplectic structure
Initialize $\mathbf{q}, \mathbf{p}$;
for $t \leftarrow 0$ ***to*** T ***by*** h **do**
  for $i \leftarrow 1$ ***to*** 4 **do**
    $\mathbf{p} \leftarrow \mathbf{p} - d_i h \nabla V(\mathbf{q})$;
    $\mathbf{q} \leftarrow \mathbf{q} + c_i h \nabla T(\mathbf{p})$;
  end for
end for
return $(\mathbf{q}, \mathbf{p})(t)$;

Algorithm 5: Yoshida Fourth-Order Symplectic Integrator

Input: System f, Jacobian $J = \partial f / \partial (n, a, Z, OX, CC)$, parameter range $\theta_5 \in [\theta_{min}, \theta_{max}]$.
Output: Critical value θ_5^* and oscillation frequency ω.

foreach θ_5 *in* $[\theta_{min}, \theta_{max}]$ **do**
  Solve $f = 0$ for steady state.
  Compute eigenvalues of J.
  Track $\max(\Re(\lambda_i))$.
  if *sign of* $\max(\Re(\lambda_i))$ *changes* **then**
    Mark $\theta_5^* \leftarrow \theta_5$,
    Compute $\omega = |\Im(\lambda)|$.
  end if
end
return (θ_5^*, ω).

Algorithm 6: Hopf Bifurcation Detection Procedure

Input: Equilibria $\{\mathbf{y}_i\}$, Jacobian $J(\mathbf{y}_i)$
Output: Hopf candidate set
for *each equilibrium* $\mathbf{y}_i$ **do**
  Compute eigenvalues λ_j of $J(\mathbf{y}_i)$;
  if $\exists$ *complex pair* $\lambda_{1,2} = \alpha \pm i\beta$ *with* $\alpha \approx 0$, $\beta \neq 0$ **then**
    Mark $\mathbf{y}_i$ as Hopf candidate;
  end if
end for
return *Hopf candidates*;

Algorithm 7: Hopf Bifurcation Candidate Identification

Input: Model parameters $(q_n, q_x, \alpha_i, \beta_i, \lambda, \delta_i, \theta_4)$, range of θ_5, step $\Delta\theta$

Output: Critical value θ_5^*, eigenvalues $\lambda_i(\theta_5)$, oscillation amplitude and frequency

Define model equations f and Jacobian $J = \partial f / \partial (n, a, Z, OX, CC)$;

foreach θ_5 *in* $[\theta_{min}, \theta_{max}]$ *with step* $\Delta\theta$ **do**

  Solve $f = 0$ for steady state using NSolve;

  Compute eigenvalues λ_i of J;

  Record $\max(\mathrm{Re}\,\lambda_i)$;

  Identify sign changes to locate Hopf intervals;

end

Refine θ_5^* via FindRoot$(\max(\mathrm{Re}\,\lambda(\theta_5)) = 0)$;

Evaluate eigenvalues at θ_5^* and estimate frequency $\omega = |\mathrm{Im}(\lambda)|$;

Simulate dynamics for $\theta_5^{\pm} = \theta_5^*(1 \pm 0.02)$ using NDSolve;

Compute oscillation amplitude and period from $a(t)$;

Generate plots: bifurcation diagram, time series, phase portraits;

Algorithm 8: Pseudocode for Hopf bifurcation detection and limit cycle analysis.